


Cite this: *RSC Adv.*, 2021, **11**, 37514

Received 5th October 2021  
Accepted 15th November 2021

DOI: 10.1039/d1ra07393a

rsc.li/rsc-advances

# Synthesis of calixresorcarenes using magnetic poly triazine-benzene sulfonamide-SO<sub>3</sub>H†

Alireza Gharehkhani, Ramin Ghorbani-vaghei<sup>ID</sup>\* and Sedigheh Alavinia

The purpose of this work is to develop a magnetically recyclable immobilized base catalyst for the green synthesis of calixresorcarenes. To achieve this, poly triazine-benzene sulfonamide (PTBSA) has been coated on magnetic Fe<sub>3</sub>O<sub>4</sub> nanoparticles and subsequently chlorosulfonic acid has been supported to obtain Fe<sub>3</sub>O<sub>4</sub>@PTBSA-SO<sub>3</sub>H. The structure of nano-Fe<sub>3</sub>O<sub>4</sub>@PTBSA-SO<sub>3</sub>H was characterized by TEM, XRD, FT-IR, VSM, WDX, EDX, TGA/DSC and FE-SEM. The catalytic efficiency of this catalyst was also investigated in the synthesis of novel calixresorcarene derivatives. The advantages of heterogeneous nature, catalytic activity and the recyclability of the polymer support were also strengthened by advanced surface treatment. These key factors (basic sites, acidic sites and heterogeneity) play essential roles in the catalyst performance. This procedure has some advantages such as short reaction time, clean and fast work-up and easy separation of the catalyst by an external magnet.

## 1 Introduction

A calixarene/calixresorcinarene is one of the most important macrocyclic molecules in materials chemistry.<sup>1</sup> This compound is the key structural fragment of fluorescent and chromogenic sensors.<sup>2</sup> Calixarene and its derivatives demonstrate numerous biological activities such as, anti-infective, antibacterial, anti-tumour and antifungal.<sup>3</sup> Moreover, many researchers have concentrated on the phase transfer catalyst activity,<sup>4</sup> encapsulation,<sup>5</sup> and supramolecular chemistry of calix[4]arene and its derivatives.<sup>6</sup> The functionalization of calix[4]arene has attracted considerable interest,<sup>7</sup> from characterization such as the ease of functionalization or modification, the flexibility and rigidity of the four different three dimensional conformations.<sup>3</sup> For the synthesis of various calixarenes/calixresorcarenes, the reaction of resorcinol with benzaldehyde derivatives is a particularly important method.<sup>8</sup> Despite the existence of this synthetic method, the synthesis of these structures by the above-mentioned routes has some drawbacks such as multi-step synthetic operation, low product yield, inaccessible starting materials, limited scope and using a homogeneous catalyst.

Homogeneous catalysts function in the same phase as reactants but heterogeneous or heterogenized ones react in a different phase. With respect to the reaction medium, the advantage of heterogeneous catalysts compared to homogeneous ones is that the former function in a different phase leading to cheap and easy separation.<sup>9</sup> Magnetic nanoparticles

(MNPs) have recently been developed as a very useful type of supported catalyst because of their easy synthesis and functionalization, good stability, high surface area, low toxicity and low price as well as facile separation using magnetic forces.<sup>10</sup> Also, to bridge the gap between heterogeneous and homogeneous catalysis, surface functionalization of magnetic particles can be considered to be a good method.<sup>11</sup>

Surface modification of heterogeneous support with polymer have attracted much attention of researchers due to its remarkable catalytic efficiency in organic synthesis which addresses the sustainability concerns including ease of recyclability, high capacity chelating, excellent chemical and thermal stability.<sup>12</sup> Thus, the application of magnetic nanoparticles and polymers as attractive candidates is currently a subject of interest in chemical processes and organic reaction.<sup>13</sup>

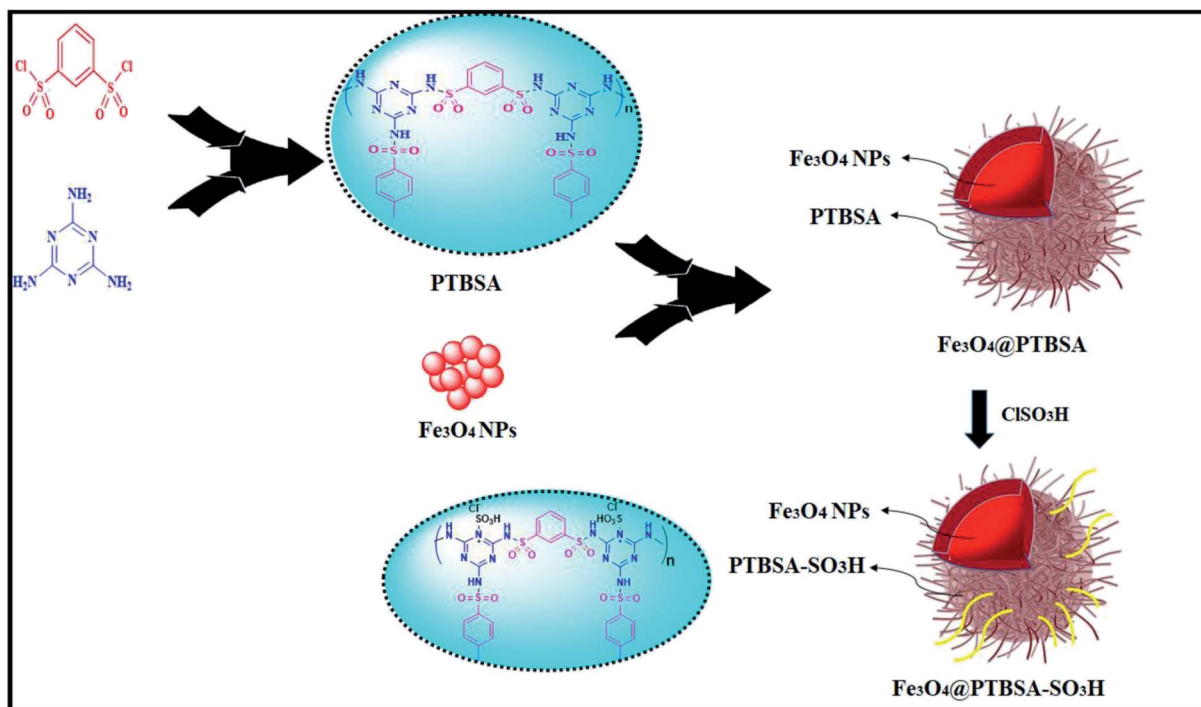
Many of the organic reactions can be performed in the presence of acidic catalysts. These catalysts generally are classified into two groups: homogeneous and heterogeneous acidic catalysts. Homogeneous acids are hazardous in handling, damaging the plant and environment through their corrosiveness, add process difficulties using quenching and separation stages, which led to the large volume of toxic and corrosive wastes. Consequently, in recent years there has been developed a great interest in using heterogeneous acid catalysts instead of those homogeneous acid catalysts, because of the possibility for recovering and recycling solids, and therefore significantly reducing the environmental impact.<sup>14</sup>

There are numerous organic and inorganic materials which can be used as supporting reagents to produce heterogeneous catalysts such as polymers,<sup>15</sup> carbons,<sup>16,17</sup> zeolites,<sup>18,19</sup> silica,<sup>20</sup> hydroxyapatite,<sup>21,22</sup> zirconia,<sup>23</sup> magnetite nanoparticle,<sup>24</sup> alumina<sup>25</sup> and *etc.* Consequently, progress in heterogeneous

Department of Organic Chemistry, Faculty of Chemistry, Bu-Ali Sina University, Zip Code 65174, Hamedan, Iran. E-mail: rgvaghei@yahoo.com; Tel: +98 81 38380647

† Electronic supplementary information (ESI) available: Detailed experimental procedure and FT-IR and MS of all compounds. See DOI: 10.1039/d1ra07393a





Scheme 1 The general route for the synthesis of Fe<sub>3</sub>O<sub>4</sub>@PTBSA-SO<sub>3</sub>H.

solid acid catalysts as a fundamental principle in green chemistry is expected to have a major impact on industrial applications as well as on scientific aspects.

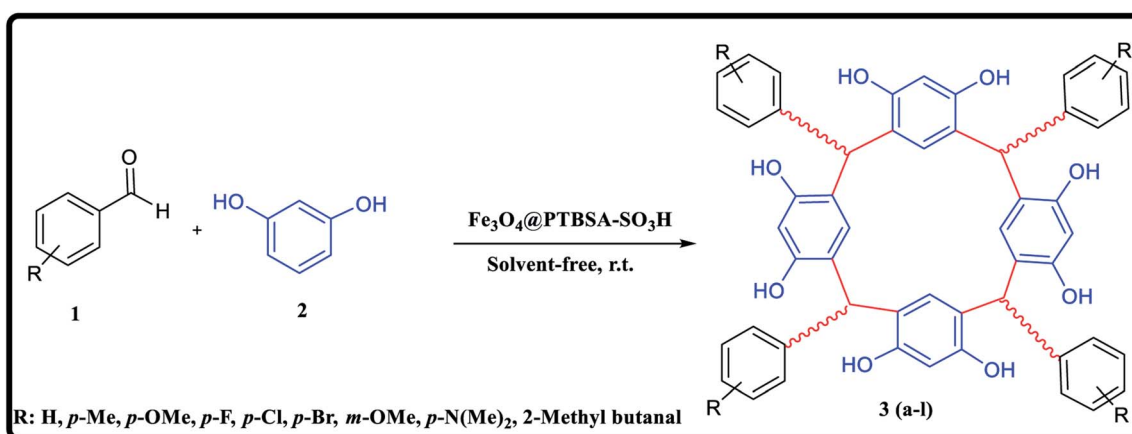
In view of the green chemistry, we tried in this work to substitute harmful mineral acids by magnetic polysulfonamide nanocomposite which contains high surface density functional group (SO<sub>3</sub>H groups). In continuation of our previous effort on the synthesis of heterogeneous polysulfonamide-based catalyst,<sup>26</sup> we have been encouraged to develop a unique nanocatalyst Fe<sub>3</sub>O<sub>4</sub>@PTBSA-SO<sub>3</sub>H by immobilization of chlorosulfonic acid over the PTBSA grafted magnetic Fe<sub>3</sub>O<sub>4</sub> NP (Scheme 1) and employed it in the green synthesis of calixresorcarenes (Scheme 2). The presence of chlorosulfonic acid as a strongly basic material efficiently promotes the reaction.<sup>27</sup>

In order to take advantage of the high surface area, high coordination group and easy magnetic reusability, Fe<sub>3</sub>O<sub>4</sub> MNP grafted PBTSA was used as the base matrix. To the best of our knowledge, there is no report hitherto on the catalytic green synthesis of calixresorcarenes using magnetic-polysulfonamide based nanocomposite.

## 2 Experimental section

### 2.1. Material and methods

All reagents and materials used in this work were of analytical reagent grade. Iron(III) chloride hexahydrate [FeCl<sub>3</sub>·6H<sub>2</sub>O, ≥98%], iron(II) chloride tetrahydrate [FeCl<sub>2</sub>·4H<sub>2</sub>O, ≥98%], melamine [1,3,5-triazine-2,4,6-triamine, ≥98%], ammonia



Scheme 2 Synthesis of calixresorcarenes derivatives using Fe<sub>3</sub>O<sub>4</sub>@PTBSA-SO<sub>3</sub>H.



solution,  $\geq 25\%$ ], [chlorosulfonic acid,  $\geq 99\%$ ], [resorcinol  $\geq 99\%$ ], were purchased from Sigma-Aldrich (Germany). Melting points were measured with open capillary tubes in the device BUCHI 510. Infrared (IR) spectroscopy was conducted on a PerkinElmer GX FT-IR spectrometer. Nuclear magnetic resonance spectra have been reported in DMSO- $d_6$  with ppm chemical displacement. Mass spectrometer was recorded in a spectrometer Shimadzu QP 1100 BX. The thermal properties of the samples were conducted using a thermogravimetric analyzer (TGADSC/Mettler Toledo) ranging from room temperature to  $600\text{ }^\circ\text{C}$  at a rate of  $10\text{ }^\circ\text{C min}^{-1}$  under  $\text{N}_2$  atmosphere.

## 2.2. Preparation of $\text{Fe}_3\text{O}_4$ MNPs

First,  $\text{FeCl}_3 \cdot 6\text{H}_2\text{O}$  (5.83 g) and  $\text{FeCl}_2 \cdot 4\text{H}_2\text{O}$  (2.147 g) were dissolved in 100 mL of deionized water and subjected to magnetic stirring at  $80\text{ }^\circ\text{C}$  for 10 min. Then 10 mL of ammonia solution (25% aqueous) was added to the reaction mixture for 30 min. To prepare  $\text{Fe}_3\text{O}_4$  nanoparticles, the reaction was refluxed for 10 h. Then, the suspended  $\text{Fe}_3\text{O}_4$  nanoparticles were separated by an external magnet and washed with distilled water and ethanol, and dried in an oven at  $80\text{ }^\circ\text{C}$  for 12 h.<sup>13a</sup>

## 2.3. Synthesis of poly(triazine-benzene sulfonamide) (PTBSA)

A mixture of melamine (0.7 mmol) and benzene-1,3-disulfonyl chloride (1 mmol) monomers was refluxed in dry acetonitrile (40 mL) for 12 h. The resulting PTBSA precipitate was washed with acetonitrile and subsequently dried in a vacuum oven at  $60\text{ }^\circ\text{C}$  (Scheme 1).

## 2.4. Synthesis of $\text{Fe}_3\text{O}_4$ @PTBSA nanocomposite

To 100 mL acetonitrile, a mixture of  $\text{Fe}_3\text{O}_4$  NPs (1 g) and poly(triazine-benzene sulfonamide) (1 g) was added and refluxed for 24 h.  $\text{Fe}_3\text{O}_4$ @PTBSA were separated by an external magnet, washed with acetonitrile and subsequently dried in a vacuum oven at  $60\text{ }^\circ\text{C}$  (Scheme 1).

## 2.5. Synthesis of $\text{Fe}_3\text{O}_4$ @PTBSA- $\text{SO}_3\text{H}$

In order to sulfonation of  $\text{Fe}_3\text{O}_4$ @PTBSA, 1.0 g of prepared nanocomposite was dispersed in 20 mL of dichloromethane and chlorosulfonic acid (10 mmol) was slowly added. The pre-synthesized  $\text{Fe}_3\text{O}_4$ @PTBSA- $\text{SO}_3\text{H}$  were then stirred for 24 h. The resulting catalyst ( $\text{Fe}_3\text{O}_4$ @PTBSA- $\text{SO}_3\text{H}$ ) were separated by an external magnet, washed thoroughly with dichloromethane (20 mL) and dried.

## 2.6. Preparation of calixresorcurene derivatives using $\text{Fe}_3\text{O}_4$ @PTBSA- $\text{SO}_3\text{H}$

A mixture of resorcinol (5 mmol), benzaldehyde derivatives (5 mmol), and  $\text{Fe}_3\text{O}_4$ @PTBSA- $\text{SO}_3\text{H}$  catalyst (0.2 g) was added in a mortar and pestle and ground vigorously at room temperature. After reaction completion (monitored by TLC, *n*-hexane/ethyl acetate, 10 : 4), the catalyst was separated from the reaction mixture by an external magnet and washed with hot ethanol. After solvent evaporation, the crude product was crystallized in ethanol, and the product was obtained with good efficiency.

## 2.7. Analytical data of the products

**2.7.1 2,8,14,20-Tetraphenyl-4,6,10,12,16,18,22,24-octahydroxycalix[4]-resorcurene (3a).** Colorless solid, mp >

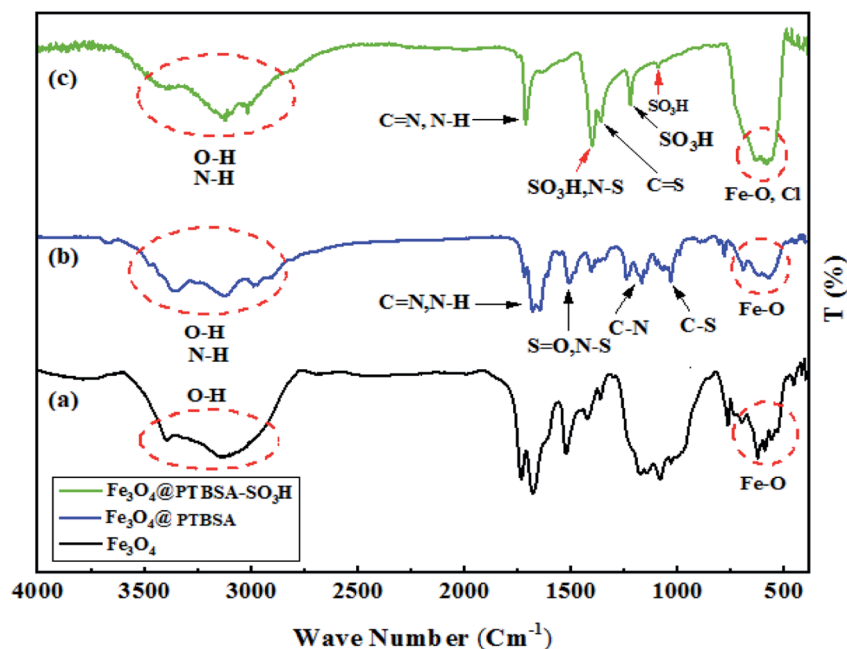


Fig. 1 FT-IR spectra of  $\text{Fe}_3\text{O}_4$  MNPs (a),  $\text{Fe}_3\text{O}_4$ @PTBSA (b), and  $\text{Fe}_3\text{O}_4$ @PTBSA- $\text{SO}_3\text{H}$  (c).



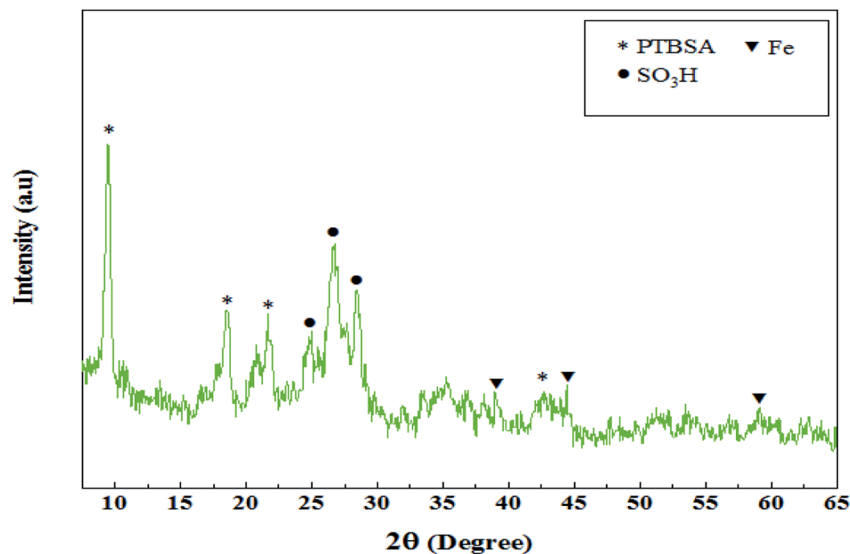


Fig. 2 XRD pattern of  $\text{Fe}_3\text{O}_4@\text{PTBSA-SO}_3\text{H}$ .

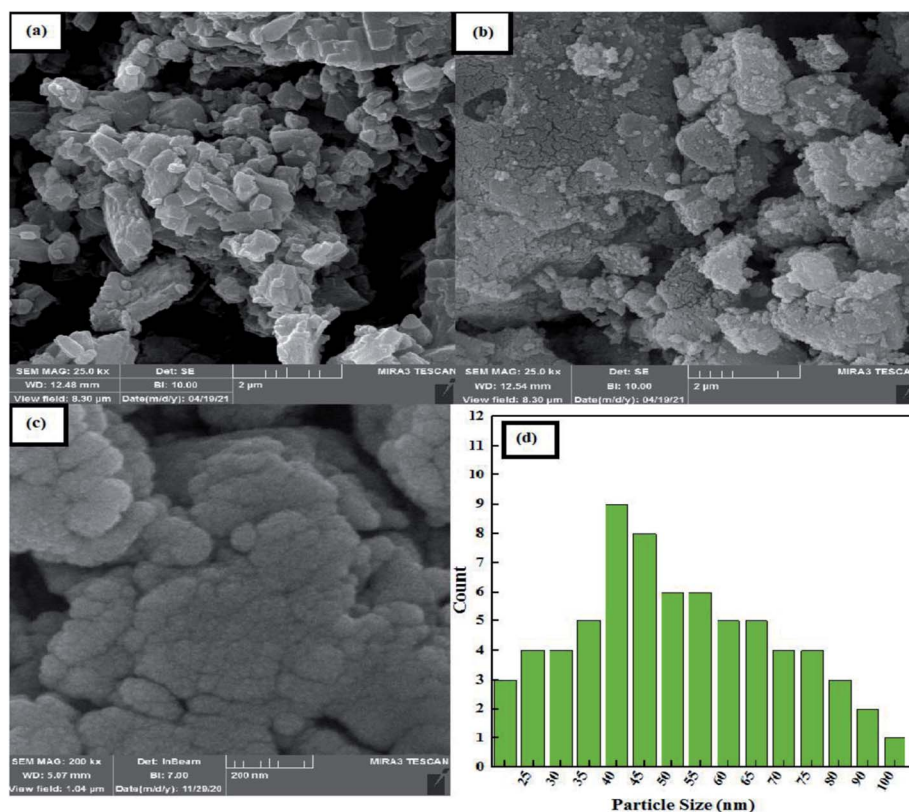


Fig. 3 FE-SEM photographs of (a) PTBSA, (b)  $\text{Fe}_3\text{O}_4@\text{PTBSA}$ , (c)  $\text{Fe}_3\text{O}_4@\text{PTBSA-SO}_3\text{H}$  and (d) particle size distribution of  $\text{Fe}_3\text{O}_4@\text{PTBSA-SO}_3\text{H}$ .

300 °C (dec); FT-IR (KBr)  $\nu$ : 3406, 3030, 2929  $\text{cm}^{-1}$ ;  $^1\text{H}$  NMR (500 MHz,  $\text{DMSO-}d_6$ )  $\delta$  ppm: 5.55 (s, 1H, CH,  $\text{H}_4$ ), 6.13 (s, 1H, Ar-H,  $\text{H}_1$ ), 6.20 (s, 1H, Ar-H,  $\text{H}_3$ ), 6.75–6.96 (m, 5H, Ar-H,  $\text{H}_5$ ,  $\text{H}_6$ ,  $\text{H}_7$ ), 8.53–8.94 (OH, broad peak,  $\text{H}_2$ , 3H), ppm.  $^{13}\text{C}$  NMR (125 MHz,  $\text{DMSO-}d_6$ )  $\delta$  ppm: 50.03, 106.94, 121.44, 127.44, 127.47, 129.03, 130.16, 144.54, 159.12.<sup>28</sup> MS:  $m/z$  = 800 [ $\text{M}^+$ ].

**2.7.2 2,8,14,20-Tetra-*p*-tolyl-4,6,10,12,16,18,22,24-octahydroxycalix[4]-resorcarene (3b).** Reddish orange solid, mp > 300 °C (dec); FT-IR (KBr)  $\nu$ : 3353, 3137, 2919  $\text{cm}^{-1}$ ;  $^1\text{H}$  NMR (500 MHz,  $\text{DMSO-}d_6$ )  $\delta$  ppm: 2.21 (s, 3H,  $\text{H}_7$ ), 5.57 (s, 1H, CH,  $\text{H}_4$ ), 6.09 (s, 1H, Ar-H,  $\text{H}_2$ ), 6.16 (s, 1H, Ar-H,  $\text{H}_3$ ), 6.37–6.97 (m, 4H, Ar-H,  $\text{H}_5$ ,  $\text{H}_6$ , 4H), 7.96–9.12 (OH, broad peak,  $\text{H}_1$ ,





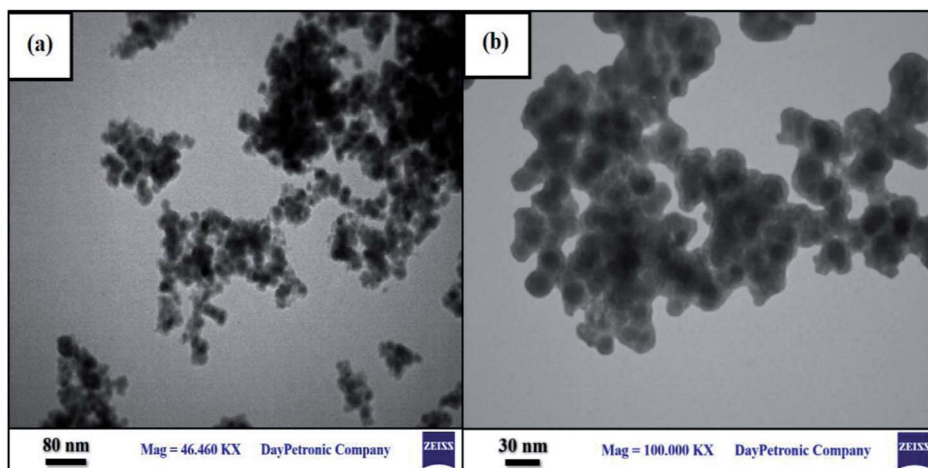


Fig. 4 TEM photographs of  $\text{Fe}_3\text{O}_4\text{@PTBSA-SO}_3\text{H}$  with the scale bar of (a) 80 nm and (b) 30 nm.

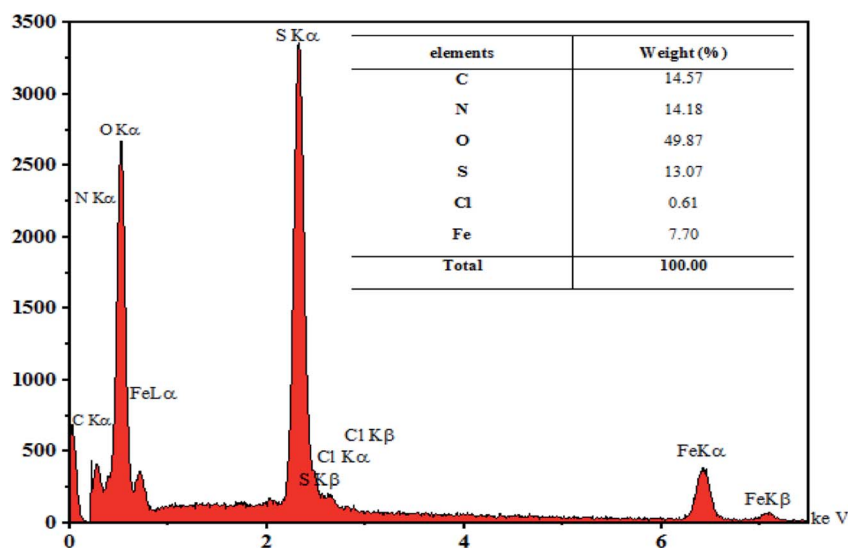


Fig. 5 EDX spectrum of  $\text{Fe}_3\text{O}_4\text{@PTBSA-SO}_3\text{H}$ .

2H), ppm.  $^{13}\text{C}$  NMR (125 MHz,  $\text{DMSO-}d_6$ )  $\delta$  ppm: 20.04, 55.75, 106.54, 121.05, 127.75, 128.86, 133.20, 143.91, 153.29.<sup>29</sup> MS:  $m/z$  = 856  $[\text{M}^+]$ .

**2.7.3 2,8,14,20-Tetra-*p*-methoxyphenyl-4,6,10,12,16,18,22,24-octahydroxycalix[4]-resorcarene (3c).** Reddish orange solid, mp > 300 °C (dec); FT-IR (KBr)  $\nu$ : 3553, 3397, 2971  $\text{cm}^{-1}$ ;  $^1\text{H}$  NMR (300 MHz,  $\text{DMSO-}d_6$ )  $\delta$  ppm: 3.71 (s, 3H,  $\text{CH}_3$  H<sub>7</sub>), 5.56 (s, 1H, CH, H<sub>4</sub>), 6.16 (s, 1H, Ar-H, H<sub>2</sub>), 6.18 (s, 1H, Ar-H, H<sub>3</sub>), 6.47–6.63 (m, 4H, Ar-H, H<sub>5</sub>, H<sub>6</sub>, 4H), 7.58–8.51 (OH, broad peak, H<sub>1</sub>, 3H), ppm.  $^{13}\text{C}$  NMR (75 MHz,  $\text{DMSO-}d_6$ )  $\delta$  ppm: 55.26, 59.35, 102.38, 106.69, 113.19, 121.22, 129.91, 138.19, 152.84, 156.96.<sup>30</sup> MS:  $m/z$  = 920  $[\text{M}^+]$ .

**2.7.4 2,8,14,20-Tetra-*p*-*N,N*-dimethylphenyl-4,6,10,12,16,18,22,24-octahydroxycalix[4]-resorcarene (3d).** Yellow solid, mp: 228–230 °C; FT-IR (KBr)  $\nu$ : 3268, 3161, 3004  $\text{cm}^{-1}$ ;  $^1\text{H}$  NMR (300 MHz,  $\text{DMSO-}d_6$ )  $\delta$  ppm: 3.02 (s, 7H,  $\text{N}(\text{CH}_3)_2$ , H<sub>7</sub>), 5.76 (s, 1H, CH, H<sub>4</sub>), 6.12 (s, 1H, Ar-H, H<sub>2</sub>), 6.21 (s,

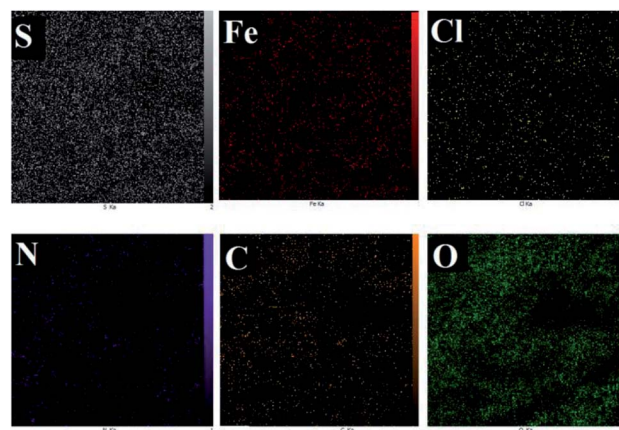
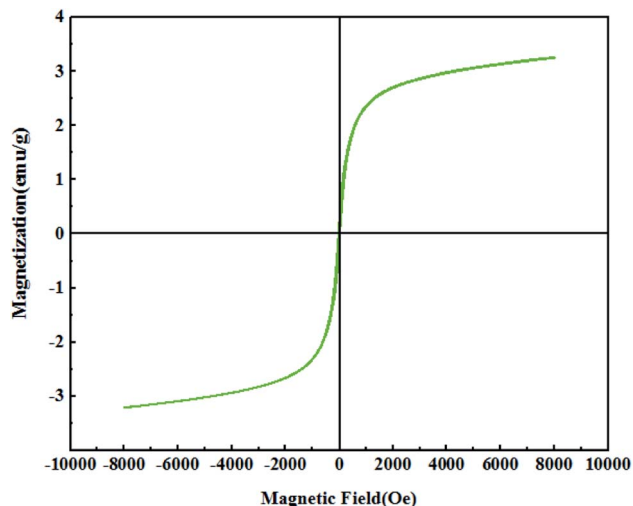
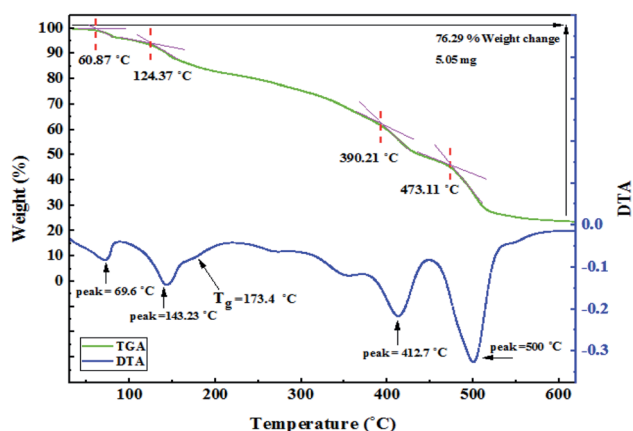


Fig. 6 Elemental mapping of  $\text{Fe}_3\text{O}_4\text{@PTBSA-SO}_3\text{H}$  shows the presence of Fe, C, N, S, Cl and O atoms in the nanocomposite.



Fig. 7 VSM analysis of  $\text{Fe}_3\text{O}_4\text{@PTBSA-SO}_3\text{H}$ .Fig. 8 TGA curve of  $\text{Fe}_3\text{O}_4\text{@PTBSA-SO}_3\text{H}$ .

$^1\text{H}$ , Ar-H,  $\text{H}_3$ ), 6.28–7.16 (m, 4H, Ar-H,  $\text{H}_5$ ,  $\text{H}_6$ , 4H), 9.89 (OH, broad peak,  $\text{H}_1$ , 4H), ppm.  $^{13}\text{C}$  NMR (75 MHz,  $\text{DMSO-}d_6$ )  $\delta$  ppm: 43.66, 56.77, 102.65, 105.89, 111.36, 117.31, 121.84, 130.47, 155.80, 156.98.<sup>31</sup>

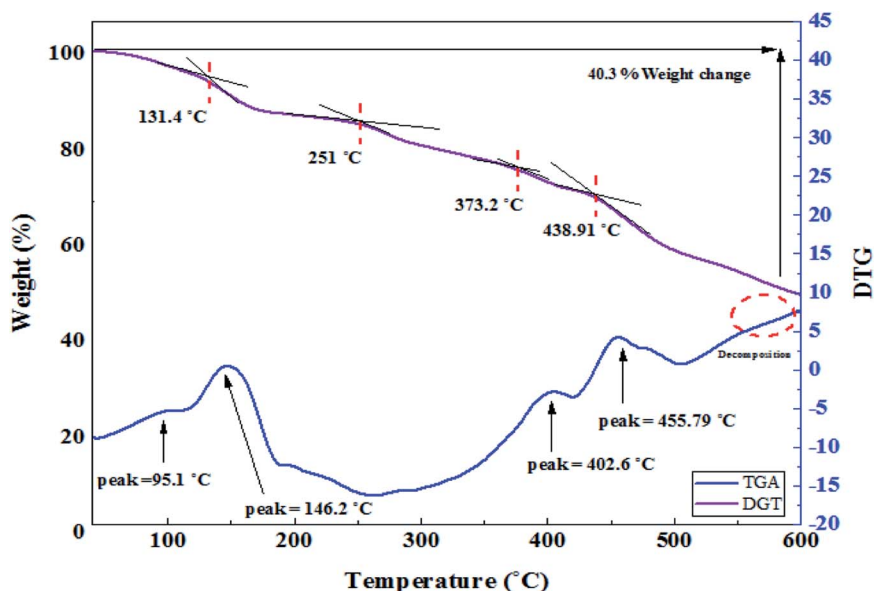
#### 2.7.5 2,8,14,20-Tetra-*m*-methoxyphenyl-

**4,6,10,12,16,18,22,24-octahydroxycalix[4]-resorcarene (3e).** Red solid, mp: 298–300 °C; FT-IR (KBr)  $\nu$ : 3403, 3059, 2926  $\text{cm}^{-1}$ ;  $^1\text{H}$  NMR (500 MHz,  $\text{DMSO-}d_6$ )  $\delta$  ppm: 3.58 (s, 3H,  $\text{OCH}_3$ ,  $\text{H}_9$ ), 5.50 (s, 1H, CH,  $\text{H}_4$ ), 6.16 (s, 1H, Ar-H,  $\text{H}_2$ ), 6.18 (s, 1H, Ar-H,  $\text{H}_3$ ), 6.50–7.70 (m, 3H, Ar-H,  $\text{H}_5$ ,  $\text{H}_6$ ,  $\text{H}_7$ ,  $\text{H}_8$ , 4H), 8.58–9.5 (OH, broad peak,  $\text{H}_1$ , 3H), ppm.  $^{13}\text{C}$  NMR (125 MHz,  $\text{DMSO-}d_6$ )  $\delta$  ppm: 54.95, 58.90, 102.39, 106.98, 110.77, 113.92, 121.66, 128.63, 147.67, 152.79, 158.90.

**2.7.6 2,8,14,20-Tetra-*p*-fluorophenyl-4,6,10,12,16,18,22,24-octahydroxycalix[4]-resorcarene (3e).** Yellow solid, mp: 223–225 °C; FT-IR (KBr)  $\nu$ : 3268, 3061, 3004  $\text{cm}^{-1}$ ;  $^1\text{H}$  NMR (500 MHz,  $\text{DMSO-}d_6$ )  $\delta$  ppm: 5.63 (s, 1H, CH,  $\text{H}_3$ ), 6.17 (s, 1H, Ar-H,  $\text{H}_5$ ), 6.18 (s, 1H, Ar-H,  $\text{H}_4$ ), 6.63–6.80 (m, 4H, Ar-H,  $\text{H}_1$ ,  $\text{H}_2$ , 4H), 8.65–9.05 (OH, broad peak,  $\text{H}_6$ , 4H), ppm.  $^{13}\text{C}$  NMR (125 MHz,  $\text{DMSO-}d_6$ )  $\delta$  ppm: 62.98, 102.78, 106.80, 114.36, 121.85, 130.20, 142.25, 158.96.<sup>32</sup> MS:  $m/z$  = 864 [M<sup>+</sup>].

**2.7.7 2,8,14,20-Tetra-*p*-bromophenyl-4,6,10,12,16,18,22,24-octahydroxycalix[4]-resorcarene (3f).** Reddish orange solid, mp: 286–288 °C; FT-IR (KBr)  $\nu$ : 3351, 3058, 2919  $\text{cm}^{-1}$ ;  $^1\text{H}$  NMR (300 MHz,  $\text{DMSO-}d_6$ )  $\delta$  ppm: 5.50 (s, 1H, CH,  $\text{H}_3$ ), 6.14 (s, 1H, Ar-H,  $\text{H}_4$ ), 6.31 (s, 1H, Ar-H,  $\text{H}_5$ ), 6.57–6.80 (m, 4H, Ar-H,  $\text{H}_1$ ,  $\text{H}_2$ ), 7.52–8.46 (OH, broad peak,  $\text{H}_6$ , 2H), ppm.  $^{13}\text{C}$  NMR (75 MHz,  $\text{DMSO-}d_6$ )  $\delta$  ppm: 65.20, 103.09, 124.29, 128.86, 130.43, 134.76, 138.08, 158.95.<sup>33</sup>

**2.7.8 2,8,14,20-Tetra-*p*-chlorophenyl-4,6,10,12,16,18,22,24-octahydroxycalix[4]-resorcarene (3g).** Reddish orange solid, mp: 286–288 °C; FT-IR (KBr)  $\nu$ : 3389, 1520, 1148  $\text{cm}^{-1}$ ;  $^1\text{H}$  NMR (300 MHz,  $\text{DMSO-}d_6$ )  $\delta$  ppm: 5.60 (s, 1H, CH,  $\text{H}_3$ ), 6.20 (s, 1H, Ar-H,  $\text{H}_4$ ), 6.33 (s, 1H, Ar-H,  $\text{H}_5$ ), 6.60 (broad peak, 2H, Ar-H,  $\text{H}_1$ ), 6.69

Fig. 9 DSC analysis of  $\text{Fe}_3\text{O}_4\text{@PTBSA-SO}_3\text{H}$ .

(broad peak, 2H, Ar-H, H<sub>2</sub>), 7.73–8.83 (OH, broad peak, H<sub>6</sub>, 3H), ppm. <sup>13</sup>C NMR (75 MHz, DMSO-*d*<sub>6</sub>) δ ppm: 62.96, 111.87, 120.13, 127.05, 127.54, 130.66, 134.00, 145.31, 153.28.<sup>34</sup>

**2.7.9 2,8,14,20-Isobutyl-4,6,10,12,16,18,22,24-octahydroxycalix[4]-resorcarene (3h).** Orange solid, mp: 286–288 °C; FT-IR (KBr) v: 3258, 2955, 2906 cm<sup>-1</sup>; <sup>1</sup>H NMR (500 MHz, DMSO-*d*<sub>6</sub>) δ ppm: 0.83 (s, 3H, CH<sub>3</sub>, H<sub>5</sub>), 0.84 (s, 3H, CH<sub>3</sub>, H<sub>8</sub>), 1.37 (m, 1H, H<sub>6</sub>), 1.67 (m, 2H, H<sub>7</sub>), 6.14 (s, 1H, Ar-H, H<sub>4</sub>, 10 Hz), 6.19–6.21 (m, 2H, Ar-H, H<sub>1</sub>, H<sub>3</sub>), 8.91 (OH, broad peak, H<sub>1</sub>, 3H), ppm. <sup>13</sup>C NMR (125 MHz, DMSO-*d*<sub>6</sub>) δ ppm: 15.48, 23.28, 26.19, 32.90, 44.47, 103.09, 122.94, 130.18, 159.19. MS: *m/z* = 712 [M<sup>+</sup>].

## 3 Results and discussion

### 3.1. Analysis of catalyst characterization data

Fig. 1 represents the FTIR spectra of the samples. According to the results of the spectrum pattern, Fe–O vibrations have been observed in the wavelength of 427–627 cm<sup>-1</sup>. The signals at around 3239 cm<sup>-1</sup> are related to vibrations of O–H functional groups (Fig. 1a). After modification of Fe<sub>3</sub>O<sub>4</sub> NPs with PTBSA, the presence of new bands appeared at around 1115 and 1181 cm<sup>-1</sup> are attributed to the stretching vibrations of C–S and C–N in the polymer, respectively. Also, the absorption vibrational bands at 1650 and 1693 cm<sup>-1</sup> related to the N–H and C=N bands of the polymer. In addition, the vibration of N–S, S=O bands was found at 1528 cm<sup>-1</sup> and the broad absorption band between 3339–33 590 cm<sup>-1</sup> is mainly due to the N–H and O–H bonds (Fig. 1b). These approved the successful

modification of Fe<sub>3</sub>O<sub>4</sub> MNPs with PTBSA. In the case of Fe<sub>3</sub>O<sub>4</sub>@PTBSA-SO<sub>3</sub>H, new adsorption bands related to chlorine and SO<sub>3</sub>H as well as all the above characteristic absorption bands were observed in the nanocomposite structure (Fig. 1c).

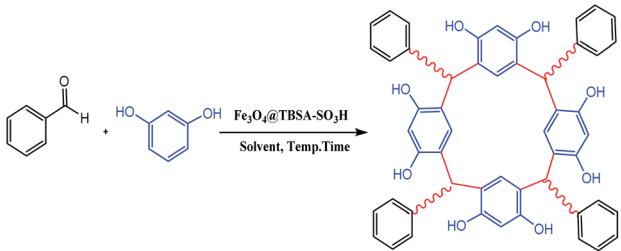
The XRD pattern of Fe<sub>3</sub>O<sub>4</sub>@PTBSA-SO<sub>3</sub>H is shown in Fig. 2. The XRD spectrum of Fe<sub>3</sub>O<sub>4</sub>@PTBSA-SO<sub>3</sub>H sample contains all characteristic peaks of both Fe<sub>3</sub>O<sub>4</sub> NPs, polymer and chlorosulfonic acid, which is indicative of the successful combination and simultaneous presence of both organic and inorganic phases in the nanocomposite texture. Three distinct peak values observed at 2θ angle are 38.9°, 44.4°, and 60°, which are also related to the Fe<sub>3</sub>O<sub>4</sub> MNPs.<sup>13b</sup> The diffraction peaks at 2θ angles of 25°, 26.7° and 28.4° confirmed the presence of SO<sub>3</sub>H groups.<sup>35</sup> Additionally, the peak observed at 42.65°, 18.5°, 9.45° and 21.65° is attributed to the PTBSA.<sup>36</sup> Through the Scherrer formula, the average particle size is found to be 6.81 nm (Fig. 2).

The surface morphologies of the samples were observed by the FESEM technique and are shown in Fig. 3. The bulk polymer structure of the pure PTBSA is given in Fig. 3a; the soft, polymeric surface of the TBSA is well visible. Surface morphologies of the Fe<sub>3</sub>O<sub>4</sub>@PTBSA and Fe<sub>3</sub>O<sub>4</sub>@PTBSA-SO<sub>3</sub>H are shown in Fig. 3b and c. The formation of sub-micrometer-sized poly TBSA and the presence of Fe<sub>3</sub>O<sub>4</sub> NPs on the surface of the Fe<sub>3</sub>O<sub>4</sub>@PTBSA and Fe<sub>3</sub>O<sub>4</sub>@PTBSA-SO<sub>3</sub>H can be observed, indicating the growth and formation of PTBSA after surface modification of Fe<sub>3</sub>O<sub>4</sub> MNPs. The simultaneous presence of both Fe<sub>3</sub>O<sub>4</sub> MNPs and polymer matrix can be observed in the FESEM images of Fe<sub>3</sub>O<sub>4</sub>@PTBSA and Fe<sub>3</sub>O<sub>4</sub>@PTBSA-SO<sub>3</sub>H nanocomposite (Fig. 3b and c), indicating the successful combination of Fe<sub>3</sub>O<sub>4</sub> core and PTBSA polymeric matrix for preparation of nanocomposite structure. According to the Fe<sub>3</sub>O<sub>4</sub>@PTBSA-SO<sub>3</sub>H particle size distribution, most particles are 40 nm (Fig. 3d). Also, the images obtained from TEM image are shown, that the nanocatalyst Fe<sub>3</sub>O<sub>4</sub>@PTBSA-SO<sub>3</sub>H has a core-shell structure and a uniform spherical morphology of 30 nm (Fig. 4).

Fe<sub>3</sub>O<sub>4</sub>@PTBSA-SO<sub>3</sub>H was analysed using EDX as shown in Fig. 5. The presence of Fe, O, N, S and Fe signals in Fig. 5 indicates that the iron oxide particles are coated with PTBSA. The characteristic peak of Cl in Fig. 5 indicate that the Fe<sub>3</sub>O<sub>4</sub>@PTBSA have been immobilized with chlorosulfonic acid.

According to this analysis, we conclude that Fe<sub>3</sub>O<sub>4</sub>@PTBSA-SO<sub>3</sub>H has been successfully synthesized. Elemental mapping images of nano-Fe<sub>3</sub>O<sub>4</sub>@PTBSA-SO<sub>3</sub>H, shows the elements of Cl, C, N, Fe, S and O in the framework of catalyst with a uniform distribution (Fig. 6).

Table 1 Optimization of reaction conditions



Entry	Cat. (g)	Solvent	Temperature (°C)	Time (min)	Yield <sup>a</sup> (%)
1	—	Solvent-free	R.T.	5	N.R
2	0.05	Solvent-free	R.T.	5	Trace
3	0.1	Solvent-free	R.T.	5	48
4	0.15	Solvent-free	R.T.	5	70
5	0.2	Solvent-free	R.T.	5	92
6	0.25	Solvent-free	R.T.	5	92
7	0.2	EtOH	R.T.	5	Trace
8	0.2	DMF	R.T.	5	Trace
9	0.2	Toluene	R.T.	5	Trace
10	0.2	CH <sub>3</sub> CN	R.T.	5	Trace
11	0.2	Solvent-free	50 °C	5	88

<sup>a</sup> Isolated yield.

Table 2 Comparison study on the catalytic efficiency of variety of catalysts with different surface modifications

Catalyst	Yield (%)	Time (min)
PTBSA-SO <sub>3</sub> H	75	5
PTBSA	68	5
Fe <sub>3</sub> O <sub>4</sub> NPs	16	5
Fe <sub>3</sub> O <sub>4</sub> @PTBSA	83	5
Fe <sub>3</sub> O <sub>4</sub> @PTBSA-SO <sub>3</sub> H	92	5



Table 3 Synthesis of calixresorcarenes using Fe<sub>3</sub>O<sub>4</sub>@PTBSA-SO<sub>3</sub>H.<sup>a</sup>

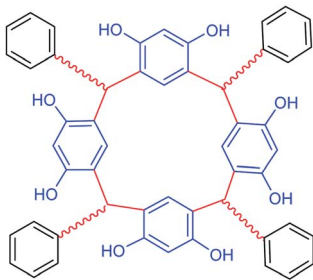
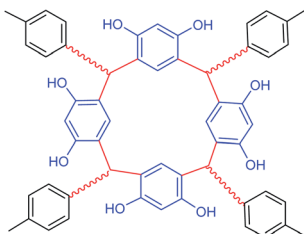
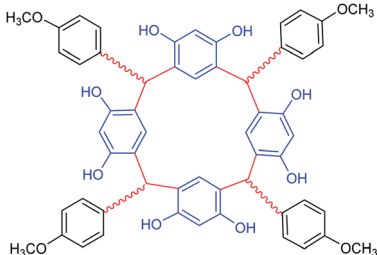
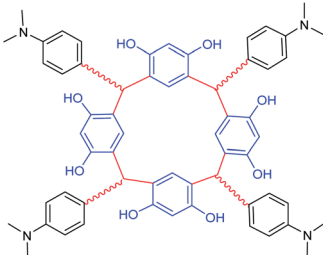
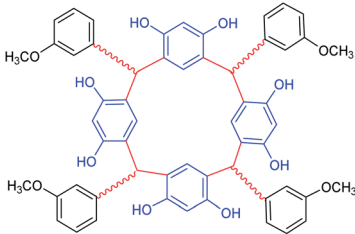
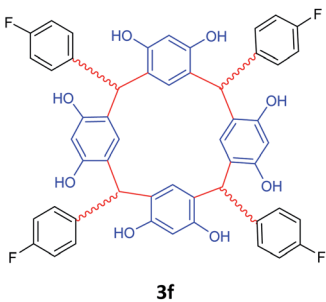
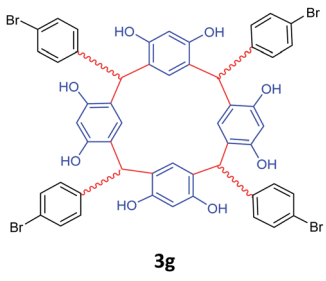
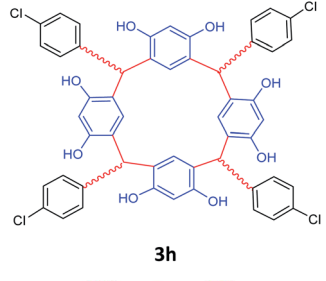
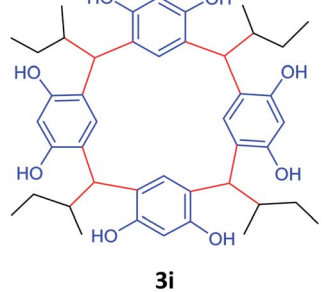
Entry	Substrate	Product <sup>a</sup>	Time (min)	Yield <sup>b</sup> (%)
1	Benzaldehyde	 <b>3a</b>	5	92
2	<i>p</i> -Methylbenzaldehyde	 <b>3b</b>	5	95
3	<i>p</i> -Methoxybenzaldehyde	 <b>3c</b>	5	98
4	4-(Dimethylamino)benzaldehyde	 <b>3d</b>	5	90
5	<i>m</i> -Methoxybenzaldehyde	 <b>3e</b>	5	88





Table 3 (Contd.)

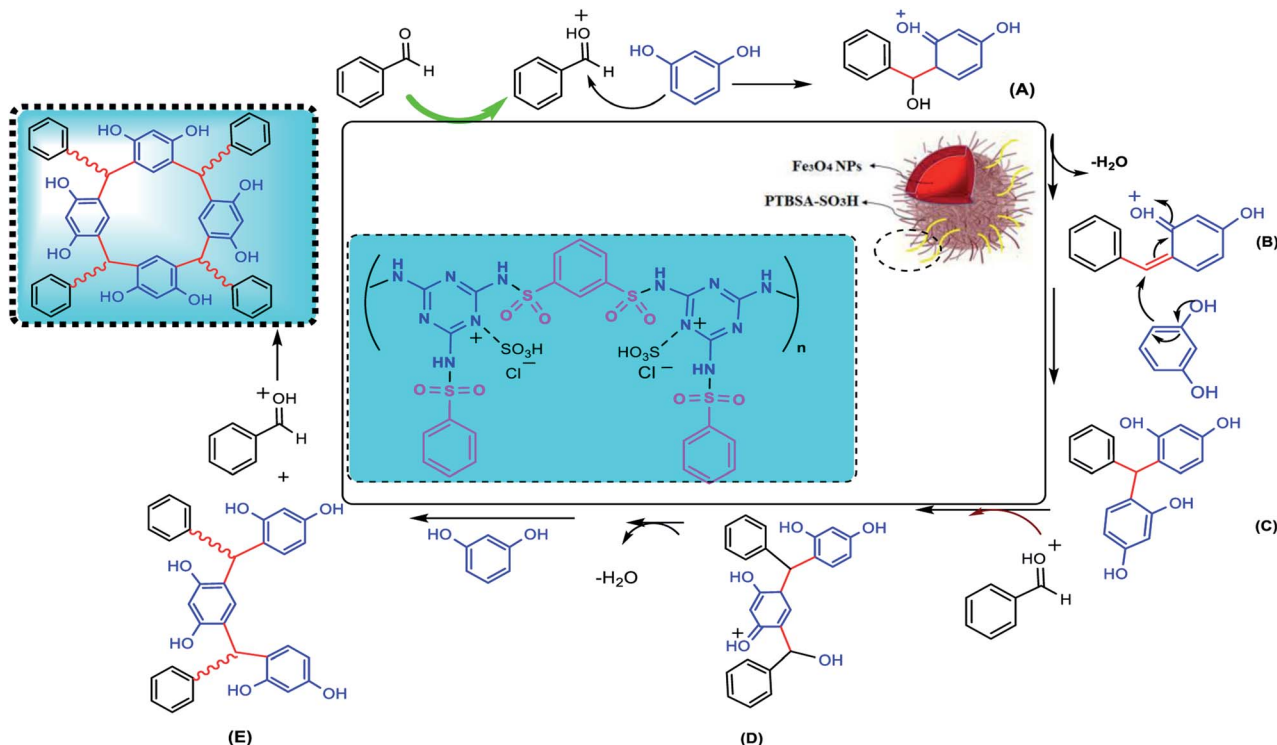
Entry	Substrate	Product <sup>a</sup>	Time (min)	Yield <sup>b</sup> (%)
6	<i>p</i> -Fluorobenzaldehyde	 3f	5	83
7	<i>p</i> -Bromobenzaldehyde	 3g	5	80
8	<i>p</i> -Chlorobenzaldehyde	 3h	5	85
9	2-Methylbutanal	 3i	5	76

<sup>a</sup> Reaction condition: benzaldehyde derivatives (5 mmol), resorcinol (5 mmol), and Fe<sub>3</sub>O<sub>4</sub>@PTBSA-SO<sub>3</sub>H (0.2 g) at room temperature. <sup>b</sup> Isolated yield.

Fig. 7 shows the magnetic properties of the catalyst as determined using VSM. According to the figure, the amount of saturated magnetization ( $M_s$ ), coercivity field ( $H_c$ ), remanent magnetization ( $M_r$ ) for Fe<sub>3</sub>O<sub>4</sub>@PTBSA-SO<sub>3</sub>H are 3.26 emu g<sup>-1</sup>, 30 Oe and 0.26 emu g<sup>-1</sup>, respectively. Also, due to the s-shape of the curve and the  $H_c$  values, the synthesized materials are supermagnetic. The value is quite reduced from the bare unmodified ferrite NPs due to the surface functionalization by SO<sub>3</sub>H groups and the polysulfonamide around it.<sup>13b</sup>

Thermal properties of the nanocomposite were investigated by thermal gravimetric analysis (TGA) and differential scanning calorimetry (DSC). The TGA curve of Fe<sub>3</sub>O<sub>4</sub>@PTBSA-SO<sub>3</sub>H shows the mass loss of the organic materials as they decompose upon heating (Fig. 8). TGA curve of Fe<sub>3</sub>O<sub>4</sub>@PTBSA-SO<sub>3</sub>H can be divided into several regions corresponding to different mass loss ranges. The first region, situated below 200 °C, displays a mass loss that is attributed to loss of trapped water or adsorbed solvent from the catalyst. The weight loss at higher temperature can be mainly ascribed to the evaporation and





Scheme 3 The plausible mechanism for the synthesis of calixresorcarenes using  $\text{Fe}_3\text{O}_4@\text{PTBSA-SO}_3\text{H}$ .

subsequent decomposition organic groups. Thus, the catalyst is stable up to  $600^\circ\text{C}$ , establishing that it could be safely used in organic reactions at temperatures in the region of  $200^\circ\text{C}$ . According to Fig. 8, as mentioned, the material is decomposed in 4 steps. In the first stage at  $60.87^\circ\text{C}$ , the second stage at  $124.37^\circ\text{C}$ , the third stage at  $390.21^\circ\text{C}$  and finally at  $473.11^\circ\text{C}$ , it loses 76.29% of its weight. The glass transition occurs at  $173^\circ\text{C}$ . According to TG/DSC analysis,  $\text{Fe}_3\text{O}_4@\text{PTBSA-SO}_3\text{H}$  nanocomposite is decomposed in 4 steps. In the first stage at  $131.4^\circ\text{C}$ , the second stage at  $251^\circ\text{C}$ , the third stage at  $373.2^\circ\text{C}$  and finally at  $438.9^\circ\text{C}$ , it loses 40.3% of its weight (Fig. 9).

### 3.2. Titration for the determination of $\text{SO}_3\text{H}$ group density

In order to compare the synthesized catalyst with the literature reported magnetic catalysts with  $\text{SO}_3\text{H}$  group, surface density of the  $\text{SO}_3\text{H}$  groups was determined using back titration method.

According to back titration method, surface high density functional group is 12 mmol per  $\text{H}^+$  per g.

### 3.3. Catalytic studies

After the full characterization of prepared  $\text{Fe}_3\text{O}_4@\text{PTBSA-SO}_3\text{H}$  nanocomposite, we evaluated its catalytic efficiency for the synthesis of 2,8,14,20-tetraphenyl-4,6,10,12,16,18,22,24-octahydroxycalix[4]-resorcarene (**3a**). The venture was started with the optimization of the reaction conditions and thereby the influence of an array of parameters like solvents, catalysts with their loads and temperature for the model reaction. Table 1 displays the corresponding results. The reaction was not successful without the catalyst (entry 1), thus signifying its

importance. To investigate the effect of the catalyst concentration, systematic studies were carried out in the presence of various amounts of the nanocatalyst (entries 2–6). Thus, the best yield is found in the presence of just 0.2 g of  $\text{Fe}_3\text{O}_4@\text{PTBSA-SO}_3\text{H}$  (entry 5), and the use of higher amounts of catalyst up to 0.25 g does not improve the result (entry 6). Thereafter, we optimized the ideal solvent in the reaction by screening the probe in different solvents like EtOH, DMF, toluene and  $\text{CH}_3\text{CN}$  (entries 7–10). The results indicated that solvent-free condition play an important role in the reaction efficiency. Considering the model reaction at different temperature (entry 11), the room temperature is the best temperature that affects the progress of the model reaction process (entry 5).

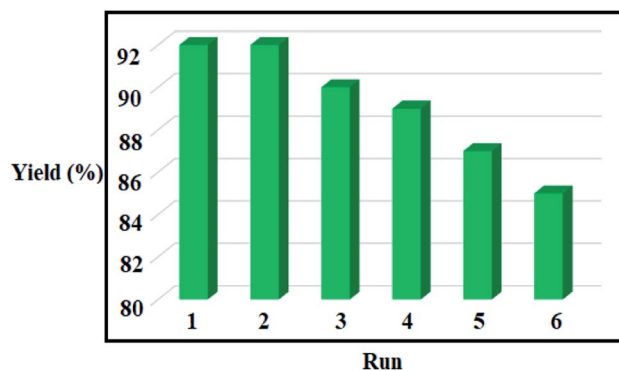


Fig. 10 Recycling of the  $\text{Fe}_3\text{O}_4@\text{PTBSA-SO}_3\text{H}$  for the reaction of benzaldehyde and resorcinol.



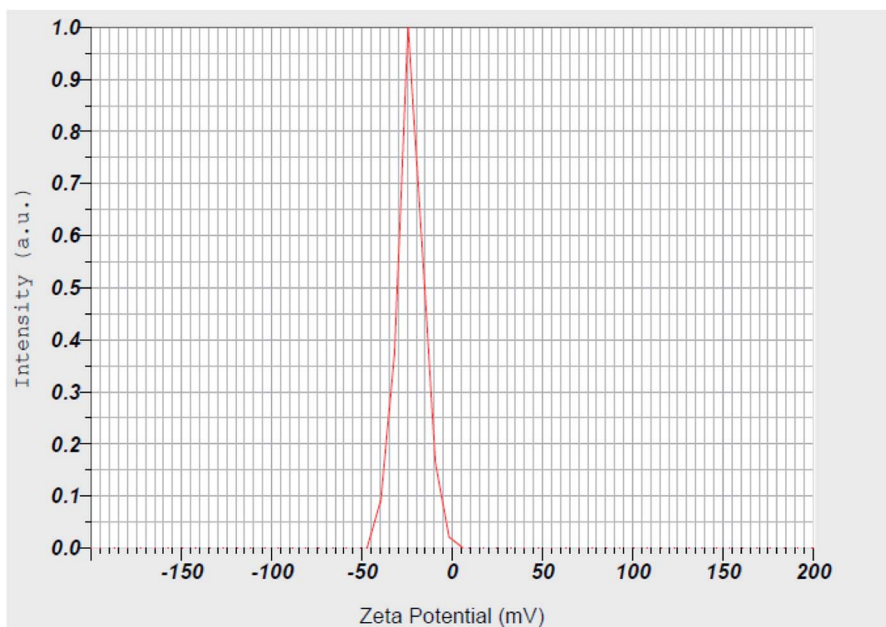


Fig. 11 Zeta potential of  $\text{Fe}_3\text{O}_4$ @PTBSA MNPs.

In order to study the effect of surface modification on the reaction progress,  $\text{Fe}_3\text{O}_4$  MNPs,  $\text{Fe}_3\text{O}_4$ @PTBSA, PTBSA- $\text{SO}_3\text{H}$  and PTBSA was used to carry out the same model reaction and none of them produced satisfactory results (Table 2). Therefore,  $\text{Fe}_3\text{O}_4$ @PTBSA- $\text{SO}_3\text{H}$  has a larger surface area for catalytic reactions and higher efficiency.

With the optimized condition in hand, we then investigated the reactions scope, not only with unsubstituted substrates but

also with a wide range of substrates bearing electron withdrawing and electron-donating functional groups. The reactions proceeded smoothly, affording calixerane derivatives in moderate to good yields (Table 3).

A probable mechanistic sequence for the formation of calixresorcarenes catalyzed by  $\text{Fe}_3\text{O}_4$ @PTBSA- $\text{SO}_3\text{H}$  is presented in Scheme 3. It is assumed that during the course of reaction, the nucleophilic addition of resorcinol to activated benzaldehyde

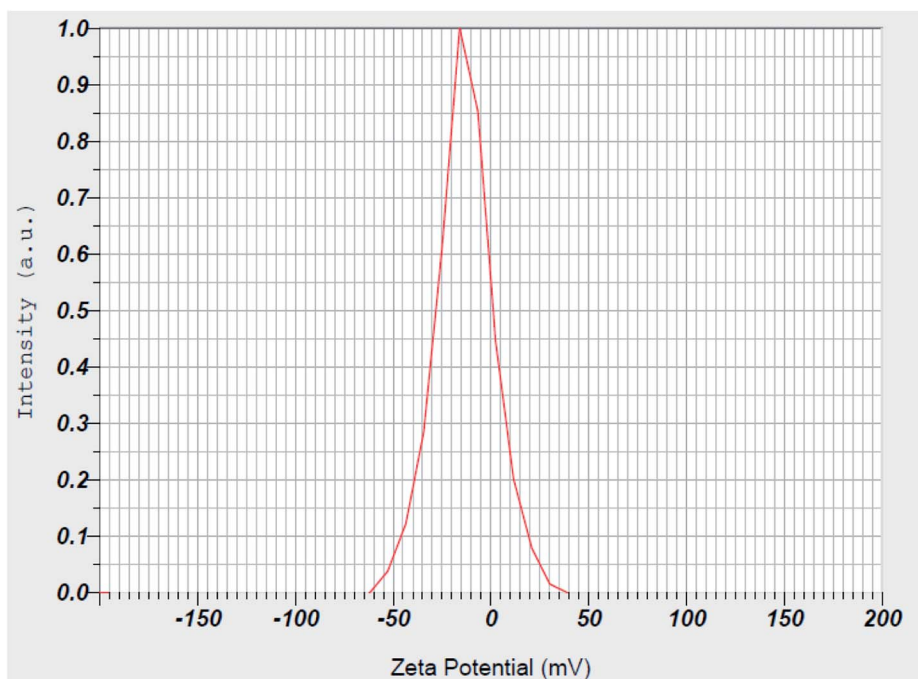


Fig. 12 Zeta potential of  $\text{Fe}_3\text{O}_4$ @PTBSA- $\text{SO}_3\text{H}$  MNPs.



**Table 4** Comparison of the present methodology with other reported catalyst for the synthesis of 2,8,14,20-tetraphenyl-4,6,10,12,16,18,22,24-octahydroxycalix[4]-resorcinarene (**3a**)

Entry	Conditions	Yield (%) [Ref]
1	Stage 1: recoreinol with hydrogenchloride in ethanol; water at 70 °C; for 1 h Stage 2: benzaldehyde in ethanol; water for 8 h; Reflux	94 (ref. 38)
2	Yttrium(III) nitrate hexahydrate in neat (no solvent) at 120 °C; for 0.25 h	92 (ref. 34)
3	Toluene-4-sulfonic acid in ethanol at 20 °C; for 1 h	85 (ref. 28)
4	Fe <sub>3</sub> O <sub>4</sub> @PTBSA-SO <sub>3</sub> H (0.2 g), grinding condition in solvent-free, R.T., 5 min	92 [this work]

by Fe<sub>3</sub>O<sub>4</sub>@PTBSA-SO<sub>3</sub>H leads to the formation of intermediate (A). By leaving the water, the intermediate A is converted to the intermediate (B), and then intermediate (C) is obtained. By performing the steps described above, the desired final product is synthesized (Scheme 3).

To explore the stability and recyclability of Fe<sub>3</sub>O<sub>4</sub>@PTBSA-SO<sub>3</sub>H, the synthesized nanocatalyst was examined for six runs in the synthesis of C-phenilcalix[4]resorcinarene (**3a**) under the optimized reaction conditions. The observed slight decrease in the activity during the sixth runs of the recycling experiments was due to the absorption/adsorption of the reactants/products in the channels or on the surface of the Fe<sub>3</sub>O<sub>4</sub>@PTBSA-SO<sub>3</sub>H (Fig. 10) (92, 92, 90, 89, 87, 85%).

Surface charge of the prepared magnetic Fe<sub>3</sub>O<sub>4</sub>@PTBSA and Fe<sub>3</sub>O<sub>4</sub>@PTBSA-SO<sub>3</sub>H were estimated using zeta potential measurements. The zeta potentials of Fe<sub>3</sub>O<sub>4</sub> MNPs is −10.63 mV.<sup>37</sup> As shown in Fig. 10 and 11, the zeta potentials of Fe<sub>3</sub>O<sub>4</sub>@PTBSA and Fe<sub>3</sub>O<sub>4</sub>@PTBSA-SO<sub>3</sub>H are −23.0 and −13.3 mV, respectively. Zeta potential measurements indicate the successful coating of magnetite nanoparticles. The increase in the negative charge density of the Fe<sub>3</sub>O<sub>4</sub>@PTBSA is attributed to the presence of the triazine groups (Fig. 11) and the decrease in the negative charge density on the surface of Fe<sub>3</sub>O<sub>4</sub>@PTBSA is attributed to the presence of the chlorosulfonic acid groups (Fig. 12).

The efficiency of Fe<sub>3</sub>O<sub>4</sub>@PTBSA-SO<sub>3</sub>H as a catalyst for the synthesis of the model compound **3a** was compared with that of other catalysts reported in the literature (Table 4). It is clear from this table that Fe<sub>3</sub>O<sub>4</sub>@PTBSA-SO<sub>3</sub>H is a more efficient catalyst for the synthesis of calixresorcinarenes. Many SO<sub>3</sub>H groups of the catalyst provide efficient acidic sites and good catalytic activity of Fe<sub>3</sub>O<sub>4</sub>@PTBSA-SO<sub>3</sub>H. Compared to the other catalysts, Fe<sub>3</sub>O<sub>4</sub>@PTBSA-SO<sub>3</sub>H provides short reaction times, simple isolation of products, high to excellent yields, stability of the catalyst and its easy magnetic separation and re-use with no significant loss of activity.

## 4 Conclusions

The main goal of the current study was to design and synthesis of a novel magnetic polysulfonamide based nanocatalyst (Fe<sub>3</sub>-O<sub>4</sub>@PTBSA-SO<sub>3</sub>H). The synthesized sample was characterized with different instrumental techniques including FE-SEM, TEM, XRD, FT-IR, and VSM to gain an in-depth insight into the physicochemical features of the synthesized catalyst. To

evaluate the effectiveness of this material in practical use the catalytic performance of the Fe<sub>3</sub>O<sub>4</sub>@PTBSA-SO<sub>3</sub>H nanocomposite toward synthesis of novel calixresorcinarenes was monitored. The results of this study revealed that Fe<sub>3</sub>O<sub>4</sub>@PTBSA-SO<sub>3</sub>H nanocomposite can be utilized as a highly efficient catalyst for green synthesis of calixresorcinarenes.

## Conflicts of interest

The authors declare that they have no competing interests.

## Acknowledgements

We sincerely thank Bu-Ali Sina University, Center of Excellence in Development of Environmentally Friendly Methods for Chemical Synthesis (CEDEFMCS) for financial support.

## References

- (a) M. Raynal, P. Ballester, A. Vidal-Ferran and P. W. N. M. van Leeuwen, *Chem. Soc. Rev.*, 2014, **43**, 1734–1787; (b) L. Cera and C. A. Schalley, *Chem. Soc. Rev.*, 2014, **43**, 1800–1812; (c) R. Custelcean, *Chem. Soc. Rev.*, 2014, **43**, 1813–1824; (d) M. E. Carnes, M. S. Collins and D. W. Johnson, *Chem. Soc. Rev.*, 2014, **43**, 1825–1834; (e) K. J. Skilling, F. Citossi, T. D. Bradshaw, M. Ashford, B. Kellam and M. Marlow, *Soft Matter*, 2014, **10**, 237–256; (f) G. Zhang, G. Kim and W. Choi, *Energy Environ. Sci.*, 2014, **7**, 954–966; (g) H.-J. Schneider, P. Agrawal and A. K. Yatsimirsky, *Chem. Soc. Rev.*, 2013, **42**, 6777–6800; (h) S. S. Zhu, H. Staats, K. Brandhorst, J. Grunenberg, F. Gruppi, E. Dalcanele, A. Lutzen, K. Rissanen and C. A. Schalley, *Angew. Chem., Int. Ed.*, 2008, **47**, 788–792.
- (a) L. Pirondini and E. Dalcanele, *Chem. Soc. Rev.*, 2007, **36**, 695–706; (b) M. H. Düker, H. Schäfer, M. Zeller and V. A. Azov, *J. Org. Chem.*, 2013, **78**, 4905–4912.
- F. Nasuhi Pur, *Mol. Diversity*, 2016, **20**, 781–787.
- R. J. Hooley, S. M. Biroš and J. Rebek Jr, *Angew. Chem., Int. Ed.*, 2006, **45**, 3517–3519.
- J. Rebek Jr, *Angew. Chem., Int. Ed.*, 2005, **44**, 2068–2078.
- (a) H. Mansikkamäki, M. Nissinen and K. Rissanen, *Angew. Chem., Int. Ed.*, 2004, **43**, 1243–1246; (b) P. Timmerman, W. Verboom and D. N. Reinhoudt, *Tetrahedron*, 1996, **52**, 2663–2704; (c) A. Jasat and J. C. Sherman, *Chem. Rev.*, 1999, **99**, 931–967.





- 7 (a) Y. Ding, J. Jiao, B. Sun, Z. Yang, C. Lin and L. Wang, The facile preparation of *p*-(methoxy)calix[n]arenes ( $n = 6, 7$ , or  $8$ ) and their permethylated derivatives, *Chin. Chem. Lett.*, 2021, DOI: 10.1016/j.cclet.2021.05.045; (b) B. Gassoumi, M. Echabaane, F. E. Ben Mohamed, L. Nouar, F. Madi, A. Karayel, H. Ghalla, M. E. Castro, F. J. Melendez, S. Özkinalı, A. Rouis and R. B. Chaaban, *Spectrochim. Acta, Part A*, 2022, **264**, 120242; (c) C. L. Boldrini, N. Manfredi, T. Montini, L. Baldini, A. Abboto and P. Fornasiero, *Current Opinion in Green and Sustainable Chemistry*, 2021, **32**, 100534; (d) K. Jlassi, K. Eidb, M. H. Sliema, A. M. Abdullaha and M. M. Chehimi, *Data in Brief*, 2021, **35**, 106799; (e) E. Ozyilmaz, S. Ascioğlu and M. Yilmaz, *Int. J. Biol. Macromol.*, 2021, **175**, 79–86; (f) Y. Jin, K. Akagawa, T. Mutai, I. Yoshikawa and K. Kudo, *Tetrahedron*, 2021, **88**, 132146.
- 8 (a) A. Arami, B. Karamia and S. Khodabakhshi, *J. Chin. Chem. Soc.*, 2014, **62**, 13–16; (b) B. A. Roberts, G. W. Cave, V. C. L. Raston and J. L. Scott, *Green Chem.*, 2001, **3**, 280–284; (c) S. A. Senthana and V. Alexander, *Dalton Trans.*, 2015, **44**, 14813–14822.
- 9 E. Farnetti, R. Di Monte and J. Kašpar, *Inorganic and Bio-organic Chemistry: Vol. II. Homogeneous and Heterogeneous Catalysis*, University of Trieste, Trieste, Italy, 2009.
- 10 X. Zheng, S. Luo, L. Zhang and J. P. Cheng, *Green Chem.*, 2009, **11**, 455.
- 11 J. Safari and Z. Zarnegar, *J. Mol. Catal. A: Chem.*, 2013, **379**, 269.
- 12 (a) R. J. Kalbasi, M. Kolahdoozan and M. Rezaei, *Mater. Chem. Phys.*, 2011, **125**, 784–790; (b) S. Zafari, R. Ghorbani-Vaghei and S. Alavinia, *Mater. Chem. Phys.*, 2021, **270**, 124840; (c) N. Shekarlab, R. Ghorbani-Vaghei and S. Alavinia, *Appl. Organomet. Chem.*, 2020, **34**, e5918; (d) J. Babamoradi, R. Ghorbani-Vaghei and S. Alavinia, *RSC Adv.*, 2021, **11**, 19147–19157; (e) Z. Hamidi and M. A. K. Zarchi, *Res. Chem. Intermed.*, 2018, **44**, 6995–7011.
- 13 (a) R. Ghorbani-Vaghei, S. Alavinia, Z. Merati and V. Izadkhah, *Appl. Organomet. Chem.*, 2018, **32**, e4127; (b) R. Ghorbani-Vaghei, S. Alavinia and N. Sarmast, *Appl. Organomet. Chem.*, 2018, **32**, e4127; (c) K. V. Karthik, A. V. Raghu, K. R. Reddy, R. Ravishankar, M. Sangeeta, N. P. Shetti and Ch V. Reddy, *Chemosphere*, 2022, **287**, 132081; (d) Y. V. Divyasri, Y. N. Teja, V. N. Koteswara Rao, N. C. G. Reddy, S. Mohan, M. M. Kumari and M. V. Shankar, *Nanostructured Materials for Environmental Applications*, 2021, 485–519; (e) A. V. Raghu, G. S. Gadaginamath, H. M. Jeong, N. T. Mathew, S. B. Halligudi and T. M. Aminabhavi, *J. Appl. Polym. Sci.*, 2009, **113**, 2747–2754; (f) A. V. Raghu, G. S. Gadaginamath, M. Priya, P. Seema, H. M. Jeong and T. M. Aminabhavi, *J. Appl. Polym. Sci.*, 2008, **110**, 2315–2320; (g) A. V. Raghu, G. S. Gadaginamath, N. Mathew, S. B. Halligudi and T. M. Aminabhavi, *J. Appl. Polym. Sci.*, 2007, **106**, 299–308; (h) G. T. Vidyavathi, B. V. Kumar, A. V. Raghu, T. Aravinda, U. Hani, H. C. AnandaMurthy and A. H. Shridhar, *J. Mol. Struct.*, 2021, **1249**, 131656; (i) L. H. Janardhan, J. M. Dong, K. Raghava Reddy, C. V. Reddy, T. Naveen Kumar, M. I. Ahamed and A. V. Raghu, *Int. J. Hydrogen Energy*, 2021, **46**, 3289–3301; (j) K. Kannan, D. Radhika, K. R. Reddy, A. V. Raghu, K. K. Sadasivuni, G. Palani and K. Gurushankar, *Nano Express*, 2021, **2**, 010014.
- 14 (a) E. Doustkhah, J. Lin, S. Rostamnia, C. Len, R. Luque, X. Luo, Y. Bando, K. C. W. Wu, J. Kim, Y. Yamauchi and Y. Ide, *Chem.-Eur. J.*, 2019, **25**, 1614–1635; (b) M. Fallah-Mehrjardi, A. R. Kiasat and K. Niknam, *J. Iran. Chem. Soc.*, 2018, **15**, 2033–2081; (c) M. A. Zolfigol, R. Ayazi-Nasrabadi, S. Bagheri, V. Khakyzadeh and S. Azizian, *J. Mol. Catal. A: Chem.*, 2016, **418**, 54–67.
- 15 C. Ying and B. Chulsung, *Curr. Org. Synth.*, 2011, **8**, 208–236.
- 16 K. Nakajima and M. Hara, *ACS Catal.*, 2012, **2**, 1296–1304.
- 17 H. Sharghi, P. Shiri and M. Aberi, *Beilstein J. Org. Chem.*, 2018, **14**, 2745–2770.
- 18 P. Gogoi, A. K. Dutta, S. Saikia and R. Borah, *Appl. Catal., A*, 2016, **523**, 321–331.
- 19 A. Brito, M. E. Borges and N. Otero, *Energy Fuels*, 2007, **21**, 3280–3283.
- 20 W. Long and C. W. Jones, *ACS Catal.*, 2011, **1**, 674–681.
- 21 J. Deng, L.-P. Mo, F.-Y. Zhao, L.-L. Hou, L. Yang and Z.-H. Zhang, *Green Chem.*, 2011, **13**, 2576–2584.
- 22 L. Ma'mani, M. Sheykhan, A. Heydari, M. Faraji and Y. Yamini, *Appl. Catal., A*, 2010, **377**, 64–69.
- 23 Y. Zhou, R. Huang, F. Ding, A. D. Brittain, J. Liu, M. Zhang, M. Xiao, Y. Meng and L. Sun, *ACS Appl. Mater. Interfaces*, 2014, **6**, 7417–7425.
- 24 N. Koukabi, E. Kolvari, M. A. Zolfigol, A. Khazaei, B. S. Shaghasemi and B. Fasahati, *Adv. Synth. Catal.*, 2012, **354**, 2001–2008.
- 25 M. Khoshnevis, A. Davoodnia, A. Zare-Bidaki and N. Tavakoli-Hoseini, *Synth. React. Inorg., Met.-Org., Nano-Met. Chem.*, 2013, **43**, 1154–1161.
- 26 (a) S. Alavinia and R. Ghorbani-Vaghei, *J. Phys. Chem. Solids*, 2020, **146**, 109573–109584; (b) F. Hamidi Dastjerdi, R. Ghorbani-Vaghei and S. Alavinia, *Catal. Lett.*, 2020, **150**, 3514–3522; (c) S. Alavinia, R. Ghorbani-Vaghei, J. Rakhtshah, J. Yousefi Seyf and I. Ali Arabian, *Appl. Organomet. Chem.*, 2020, **34**, e5449; (d) S. Alavinia and R. Ghorbani-Vaghei, *New J. Chem.*, 2020, **44**, 13062–13073; (e) S. Solgi, R. Ghorbani-Vaghei and S. Alavinia, *J. Porous Mater.*, 2021, **28**, 289–298; (f) N. Shekarlab, R. Ghorbani-Vaghei and S. Alavinia, *J. Organomet. Chem.*, 2021, **949**, 121971; (g) A. Rahimi, R. Ghorbani-Vaghei and S. Alavinia, *J. Porous Mater.*, 2021, **28**, 1643–1653; (h) S. Alavinia and R. Ghorbani-Vaghei, *RSC Adv.*, 2021, **11**, 29728–29740; (i) S. Alavinia and R. Ghorbani-Vaghei, *Monatsh. Chem.*, 2021, **152**, 1269–1276.
- 27 S. Solgi, R. Ghorbani-Vaghei, S. Alavinia and V. Izadkhah, Preparation and Application of Highly Efficient and Reusable Nanomagnetic Catalyst Supported with Sulfonated-Hexamethylenetetramine for Synthesis of 2,3-Dihydroquinazolin-4(1*H*)-Ones, *Polycyclic Aromat. Compd.*, 2020, DOI: 10.1080/10406638.2020.1833054.



- 28 A. M. Shebitha, S. S. Sreejith, P. B. Sherly mole, N. Mohan, G. Avudaiappan, K. Hiba, K. S. Priya and K. Sreekumar, *J. Mol. Struct.*, 2020, **1214**, 128215.
- 29 B. Karami, S. Khodabakhshi, N. Safikhani and A. Arami, *Bull. Korean Chem. Soc.*, 2012, **33**, 123–127.
- 30 A. A. Castillo-Aguirre, A. Pérez-Redondo and M. Maldonado, *J. Mol. Struct.*, 2020, **1202**, 127402.
- 31 A. Mobinikhaledi, M. Kalhor, A. R. Ghorbani and H. Fathinejad, *Asian J. Chem.*, 2010, **22**, 1103–1106.
- 32 Z. Ling-ling, W. Yu, H. Shu-ying, L. Gui-xiang, C. Liang-feng, Y. Shu-ning, Z. Wen-li and W. Hui, *Lett. Org. Chem.*, 2013, **10**, 298–301.
- 33 L. M. Tunstad, J. A. Tucker, E. Dalcanale, J. Weiser, J. A. Bryant, J. C. Sherman, R. C. Helgeson, C. B. Knobler and D. J. Cram, *J. Org. Chem.*, 1989, **54**, 1305–1312.
- 34 A. Arami, B. Karami and S. Khodabakhshi, *J. Chin. Chem. Soc.*, 2015, **62**, 13–16.
- 35 J. Safaei-Ghomi and H. Shahbazi-Alavi, *Sci. Iran.*, 2017, **24**, 1209–1219.
- 36 (a) F. Fina, S. K. Callear, G. M. Carins and J. T. Irvine, *Chemistry of Materials*, 2015, **27**, 2612–2618; (b) L. Jia, D. Wang, L. Liu, S. Zhang and T. Xu, *Des. Monomers Polym.*, 2014, **17**, 425–429.
- 37 M. A. Akl, A. M. Atta, A. E.-F. M. Yousef and M. I. Alaa, *Polym. Int.*, 2013, **62**, 1667–1677.
- 38 S. A. Senthana and V. Alexander, *Dalton Trans.*, 2015, **44**, 14813–14822.

